Available online at www.sciencedirect.com
ScienceDirect
Journal of Power Sources 174 (2007) 921–926
JOURNAL OF POWER SOURCES
www.elsevier.com/locate/jpowsour

Short communication

A novel Sn_xSbNi composite as anode materials for Li rechargeable batteries

Hong Guo, Hailei Zhao *, Xidi Jia, Jianchao He, Weihua Qiu, Xue Li

School of Materials Science and Engineering, University of Science and Technology Beijing, Beijing 100083, China

Available online 28 June 2007

Abstract

The approach of carbothermal reduction was employed to prepare the micro-sized Sn_xSbNi composites used as anode material for rechargeable lithium-ion batteries. The synthesized spherical Sn_xSbNi particles show a loose micro-sized structure and a multi-phase composition. The effect of Sn content in Sn_xSbNi on the electrochemical properties of the Sn_xSbNi composite anode was investigated. Increasing the amount of tin in Sn_xSbNi composite leads to an increase in the reversible discharge capacity, however, excessive introduction of Sn into Sn_xSbNi alloy will cause the fast capacity decline of electrode. Sn_2SbNi alloy provides a reversible specific capacity over 660 mAh g^{-1} and an initial capacity loss of 120 mAh g^{-1} with an excellent cycleability. The low initial capacity loss is attributable to the large particle size of Sn_xSbNi powders, while the excellent cycling stability is ascribed to the loose particle structural characteristics and multi-phase features. The former could accommodate the volume change of electrode, while the latter will result in a stepwise lithiation/delithiation behavior and thus a smooth volume change of electrode in cycles.

Keywords: Sn_xSbNi composite; Anode materials; Carbothermal reduction; Li-ion batteries

1. Introduction

The society's drastic dependence on oil, combined with global warming and pollution in our cities, has conspired to make renewable power source a worldwide imperative for the upcoming years. As a result, there will be a far increasing need for electrical energy storage to meet the vast supply lack resulted from nuclear energy, wind blows and the sun shines. Although the widely current used Li-ion battery is a good successful technology in conquering the battery market, the new challenges to achieve higher energy density, higher rates, higher stability, longer cycle life and improved safety stimulate the research for grand new breakthroughs in electrode materials [1–3]. Intensive worldwide attempts have been focused on Sn-based anode materials due to its extremely high lithium storage (994 mAh g^{-1} for $Li_{22}Sn_4$) [4–6]. However, the main problem to limit the commercialization of Sn-based materials is their relatively large volume expansion upon lithiation that results in mechanical disintegration of the electrode and consequent capacity fade [7,8]. Many efforts, therefore, have been devoted to improve the cycling duration of Sn-based system [9–11], which include decreasing particle size of active material to nano-scale and the use of intermetallics or composite host material instead of pure metal [12–13]. Related reports have revealed that reducing the size of active particles did not effectively improve the cycleability of the alloy materials for the case of Sn, because the nano particles are apt to aggregate, forming inactive dense blocks after several cycles [14,15]. Comparatively, the use of intermetallics or multi-phase active material instead of pure metal seems to be a more effective way to control the volume changes of the alloy electrodes [16,17], where all the active components can react with Li but at different potentials in the charging/discharging process, such as SnSb [3,6,18,19], SnAl [20,21]. In this case, the volume change occurs in a stepwise manner rather than at a certain fixed potential, thus the unreacted component can accommodate the strain yielded by the reacted phase. As a result, the geometric configuration and cycling stability of electrode are improved. Another promising effective approach is to employ active/inactive alloy or intermetallics, where the inactive component can buffer the volume change caused by the active component and thus increase the cycling stability of electrode, such as SnCu [22,23] and SnNi [16,24].

* Corresponding author. Tel.: +86 10 62334863; fax: +86 10 62332570.
E-mail address: hlzhao@mater.ustb.edu.cn (H. Zhao).

0378-7753/$ – see front matter © 2007 Elsevier B.V. All rights reserved.
doi:10.1016/j.jpowsour.2007.06.144

In present work, a strategy is adopted to combine the virtues of both active/inactive and active/active alloys to fabricate an Sn_xSbNi alloy powder with two active components and one inactive component. The two active components can realize the high capacity feature of electrode and can make the volume change of electrode take place in a stepwise manner due to the different lithiation potentials of two active components, leading to a stable cycling performance. Meanwhile, the inactive component Ni can increase the resistance of electrode to the volume change due to its excellent ductility. Though Ni shows inert with Li, its excellent flexibility and electric conductive character will contribute greatly to the cycling stability of electrode. Therefore, Sn_xSbNi alloy is expected to have high specific capacity and good cycling stability. To our best knowledge, there are no reports available on Sn_xSbNi composite used as anode for lithium-ion batteries up to present. In this work, Sn_xSbNi alloy powders with different chemical compositions were prepared by carbothermal reduction method from tin, antimony and nickel oxides for the purpose of reducing the production cost and obtaining the micro-scaled particles to decrease the initial irreversible capacity loss. The effect of chemical composition on the electrochemical properties of Sn_xSbNi electrode was investigated in terms of cyclic performance and cyclic voltammetry (CV) features.

2. Experimental

SnO_2 (99.9%, STREM Chemicals), Sb_2O_3 (99.9%, Merck), NiO (99.9%, STREM Chemicals) and carbon powder (>99%, STREM Chemicals) were used as raw materials. The mixtures of SnO_2, Sb_2O_3, NiO and C were prepared according to the following reaction:

$$2xSnO_2 + Sb_2O_3 + 2NiO + (4x+5)C \rightarrow 2Sn_xSbNi + (4x+5)CO\uparrow \quad (1)$$

where $x = 1$, 2 and 3.

After mixed and ground, the sample was calcined at 900 °C for 2 h in argon atmosphere at the heating rate of 5 °C min^{-1} in a tube furnace and then allowed to cool down naturally to room temperature inside the off-powered furnace. X-ray diffraction (XRD) was carried out to identify the phase composition of synthesized powders over the 2θ range from 10° to 90° using a Rigaku D/max-A diffractometer with Cu Kα radiation. Morphologies of the synthesized alloy powders were observed with a Hitachi S-3500N scanning electron microscope (SEM). The microcosmic particle morphology of the synthesized Sn_xSbNi was observed by transmission electron microscope (TEM, JEM-100CXII) and the corresponding lattice structure was identified by selected area electron diffraction (SAED) technique. TEM sample were dispersed in ethanol and collected on a holey micro grid supported on a copper mesh. For electrochemical performance evaluation, half-cell studies were performed. In the experimental Sn_xSbNi electrode, C (acetylene black) powder and polyvinylidene fluoride (PVDF) were used as conductive additive and binder, respectively. The synthesized Sn_xSbNi powders were mixed with acetylene black and PVDF dissolved in *N*-methyl-pyrrolidinone in the weight ratio of 80:10:10 to form slurry, which was painted on a copper foil used as current collector. After solvent evaporation, the electrode was pressed and dried at 120 °C under vacuum for 24 h.

The cells were assembled in argon filled glove-box. Metallic lithium foil was used as counter electrode. The electrolyte was 1 M $LiPF_6$ (Merck, battery grade) in a mixture of ethyl carbonate (EC) and dimethyl carbonate (DMC) (1:1 in vol. ratio). Celgard 2400 polyethylene was used as the separator. Cycling tests were carried out at the charge and discharge current density of 100 mAh g^{-1} in the voltage range of 0.01–1.5 V versus Li/Li^+ by LAND BT-10 tester (Wuhan, China). Cyclic voltammetry was performed between 0.01 and 1.7 V with scan rate of 0.05 mV s^{-1}.

3. Results and discussion

XRD patterns of the synthesized Sn_xSbNi composite powders with different atomic ratios are shown in Fig. 1.

It reveals that all the products are multi-phase compounds, which mainly consist of SnSb, Ni_3Sn_4 intermetallics and Sn, Ni metals. No peaks assignable to SnO_2, Sb_2O_3 and NiO were identified, indicating that all oxides have been reduced completely. No obvious peaks corresponding to metal Sb were found in XRD pattern, implying that most of the Sb component has combined with Sn and forms SnSb intermetallic and some other Sb may exist in amorphous state, as evidenced by the relatively high background of XRD pattern. With the increase of Sn content in Sn_xSbNi composite, the relative intensity of peaks corresponding to Sn increases gradually, indicating that a certain amount of single phase Sn exists in Sn_xSbNi composites.

The SEM images of synthesized composite powders are presented in Figs. 2–4. The synthesized powders show mainly two different particle shapes, spherical particles with a size of range from 1 to 100 μm and polygonal particles with an average size of 50 μm, respectively. According to EDS analysis, the sphere particles are Sn, Sb, Ni with a small quantity of carbon and the polygonal particles are carbon with a little amount of Sn, Sb and Ni. The size of particle is closely correlated with the content of

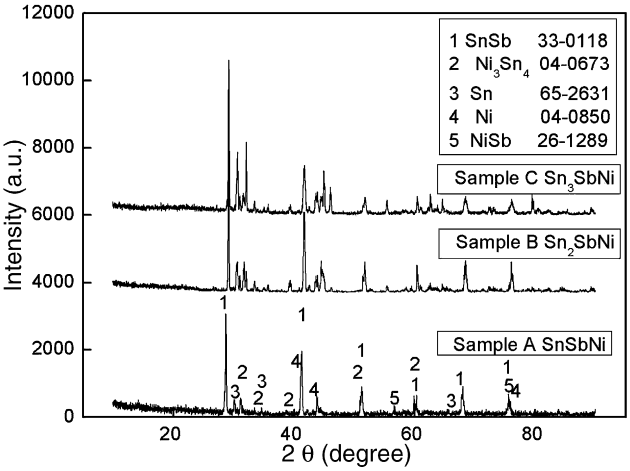

Fig. 1. XRD patterns of Sn_xSbNi composite powders with different atomic ratios.

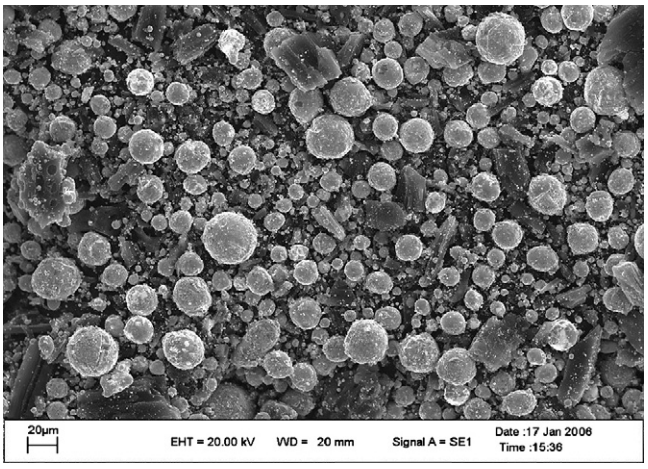

Fig. 2. SEM image of SnSbNi composite powders.

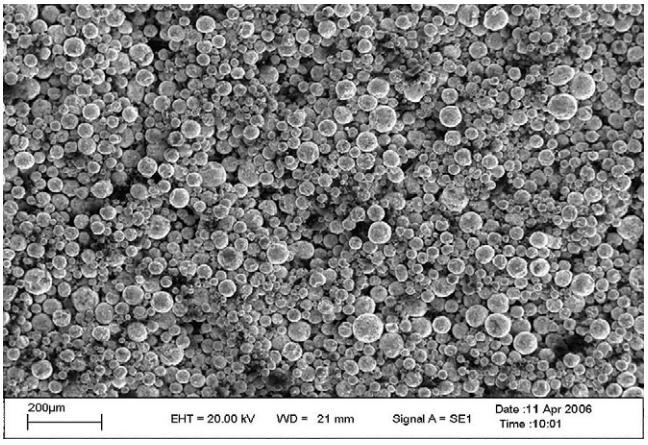

Fig. 3. SEM image of Sn_2SbNi composite powders.

Sn, i.e. the particle size of Sn_xSbNi powders increases with the Sn content. From the view point of phase diagram, the introduction of Sn will result in more liquid phase in Sn–Sb–Ni system at synthesizing temperature due to its low melting point. The liquid is apparently favorable to the mass transportation and thus grain growth, leading to large particle size of Sn_xSbNi powders.

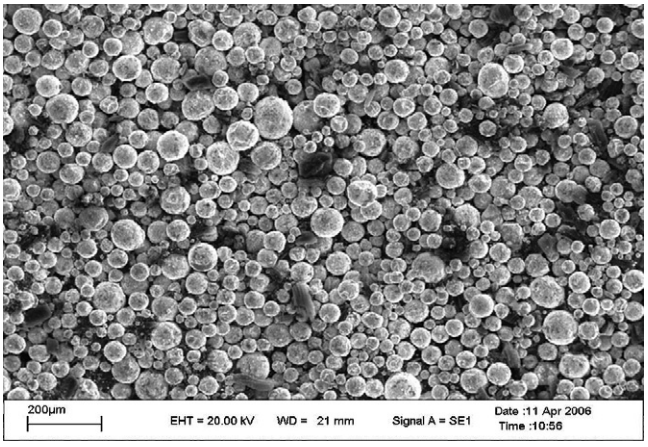

Fig. 4. SEM image of Sn_3SbNi composite powders.

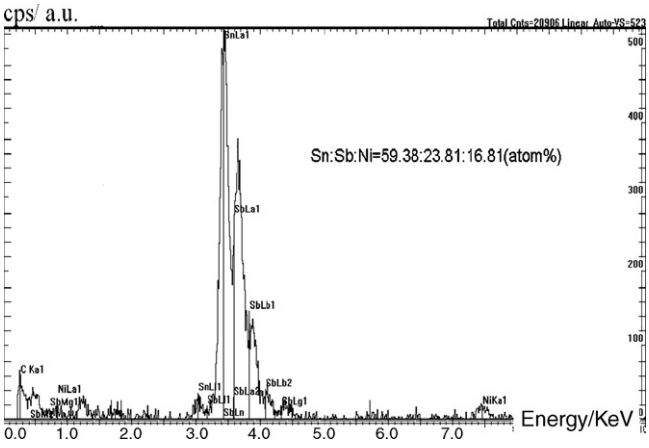

Fig. 5. EDS mapping for the area shown in Fig. 3.

The observation on the inner structure of an Sn_2SbNi particle, shown in (Fig. 6), reveals that the synthesized spherical Sn_2SbNi composite particle has a loose microstructure with obvious small opening holes among different grains. This loose structural characteristic and thus the space inside the particles can certainly help to buffer the volume changes of Sn_xSbNi alloy electrode during electrochemical reaction and hence increase the cycling stability of electrode. Furthermore, a little amount of carbon is remained in Sn_xSbNi composite powders, as shown in Figs. 2–4 and evidenced by the EDS analysis (Fig. 5). The remnant carbon is propitious to the enhancement of electronic conductivity of Sn_xSbNi composite electrode. Besides, it can accommodate in some extent the volume change caused by alloying/de-alloying of Sn and Sb with Li and can prevent particle agglomeration effectively during electrochemistry cycling [20,21]. Therefore, it will contribute greatly to the ameliorated electrochemistry performance of the Sn_xSbNi composite electrode.

EDS analysis of the synthesized Sn_2SbNi composite powders, shown in Fig. 5, gave a Sn:Sb:Ni atomic percent ratio of 59.38:23.81:16.81, showing seemingly that tin-riched composite is obtained. The chemical composition of synthesized material is somewhat deviating from the starting ratio of

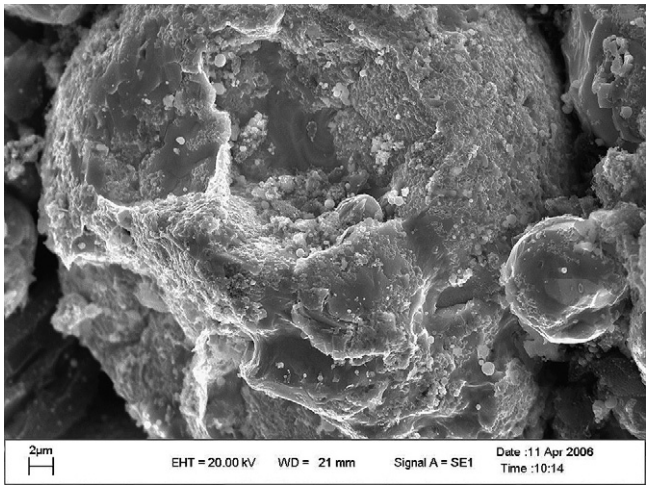

Fig. 6. Inner image of a Sn_2SbNi alloy particle.

Sn:Sb:Ni, i.e. 2:1:1 (atom ratio) before calcinations. This is considered to be resulted from the big difference in melting point between Sn, Sb and Ni. Due to its low melting point, Sn (melting point 231.81 °C) and Sb (melting point 630.59 °C) will have low viscosity and high fluidity at 900 °C and thus easily coat on the surface of some nickel contained particles having a relatively high melting point. It is difficult for EDS to detect the inner component of a coated particle; as a consequence, EDS gave a high content of Sn and Sb for the synthesized Sn_2SbNi composite powders.

Fig. 7(a) and (b) shows the TEM images of an Sn_2SbNi alloy powder prepared by carbothermal reduction. It shows a clear grain shape and the crystal edges can be observed. A multicrystal structure with clear crystal loops of diffraction and a distinct single crystalloid lattice structure can be detected by SAED, as illustrated in Fig. 7. This indicates again that the single spherical particles observed in SEM are practically aggregates of nano-sized grains.

Lithium-ions insert into and extract from Sn_xSbNi composite electrode are defined as discharge and charge processes,

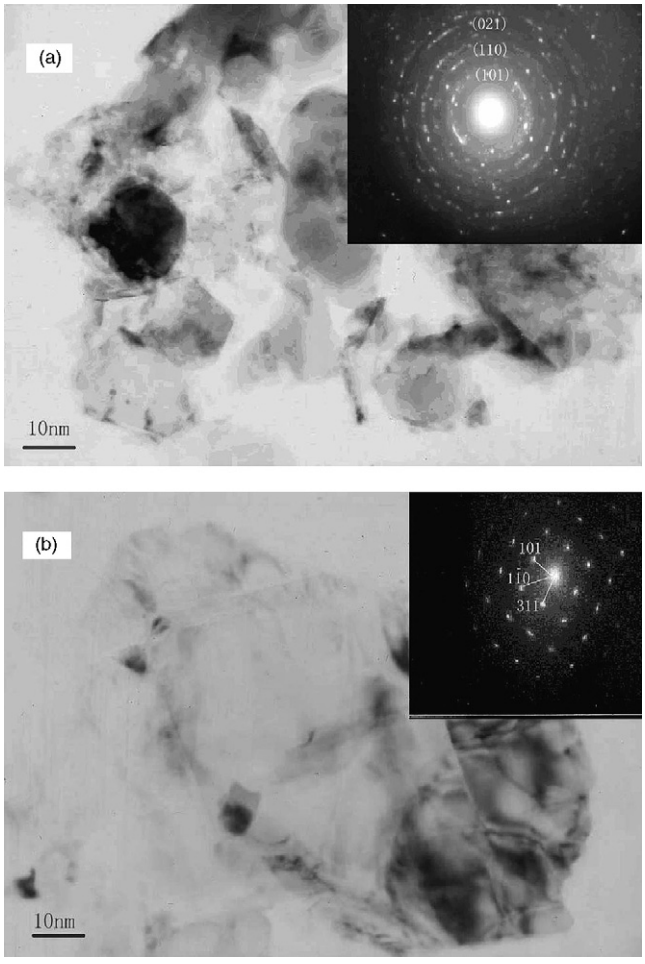

Fig. 7. TEM micrograph of Sn_2SbNi alloy powders with two different structures, multicrystalline (a) and single crystal (b). The inset in (a) is the selected area electron diffraction of an area of Sn_2SbNi alloy particle, showing multicrystalline characteristic of SnSb 04-0673. The inset in (b) is the selected area electron diffraction of another field of Sn_2SbNi alloy particle, showing the single crystalline characteristic of Sn 33-0118.

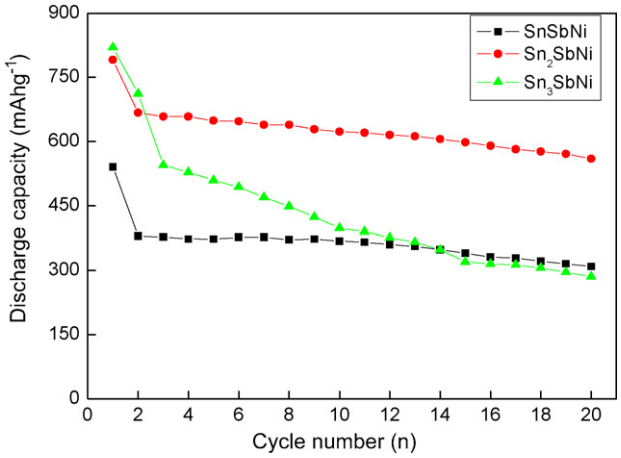

Fig. 8. Cyclic performance of Sn_xSbNi composite electrode at current density of 100 mAh g^{-1} ($x = 1$, 2 and 3).

respectively. The cyclic performance profiles of Sn_xSbNi composite electrode ($x = 1$, 2 and 3) at constant current density of 100 mAh g^{-1} are shown in Fig. 8.

The first discharge capacity of SnSbNi, Sn_2SbNi and Sn_3SbNi electrode are 540, 791 and 860 mAh g^{-1}, respectively. The increase in initial discharge capacity with the increase of Sn content is mainly attributable to the high lithium storage capacity of Sn. In the following 20 cycles, except of Sn_3SbNi, the synthesized SnSbNi and Sn_2SbNi alloy electrode exhibit good stability with discharge capacities of ~350 mAh g^{-1} and ~660 mAh g^{-1} and the columbic efficiencies of 97% and 96%, respectively. The results are understandable because of the loose particle structural and the multi-element characteristics. The former can provide space to accommodate the volume change caused by the lithiation/delithiation of electrode, while the latter allow the lithiation/delithiation of Sn_xSbNi electrode to take place at different potentials, i.e. in a stepwise behavior, thus make the volume change of electrode occur more smoothly. These will eventually result in a good structural and cyclic stability of electrode. Clearly, the inactive matrix Ni can buffer the volume change of Sn and Sb in the electrochemical cycling process thus will also contribute to the good cycleability of electrode. The dispersion of carbon in Sn_xSbNi particles is another potential reason to the good durability of composites, because it can prevent in certain extent the aggregation of the alloy particles. In addition, the good electronic conductivity of components nickel and carbon should also be responsible for the better electrochemistry performance of electrode. Unfortunately when the atomic ratio of Sn:Sb:Ni arrived at 3:1:1, the capacity of Sn_3SbNi electrode fades drastically from 712 to 285 mAh g^{-1} after 20 cycles. The relatively excessive amount of Sn in Sn_xSbNi alloy electrode will result in large volume expansion upon lithiation of electrode, which is considered to be the main reason of the poor cycling behavior of electrode. The maximal volume expansion of tin can reach as high as 300% according to the reference [22]. Another reason is that more Sn content in Sn_xSbNi composite may easily congregate together upon electrochemical cycling to form large Sn particles, which will readily result in mechanical pulverization of the electrode and consequent capacity drop of electrode.

The increased kinetic polarization of rich-tin electrode is another reason for the unstable cycleability.

The initial irreversible capacity is about 120 mAh g^{-1} for synthesized Sn_2SbNi, which is much lower than that of most reported alloy anode electrodes fabricated by liquid coprecipitation reduction [3,7,13,16]. The improvement in initial irreversible capacity is attributed to the relatively large particle size and thus low specific surface area of Sn_xSbNi alloy powders. The low specific surface area resulted from the large-sized particles of Sn_xSbNi will lead to low surface impurity, especially oxides, which is believed to be one of the main origins of the irreversible capacity [5]. Furthermore, the lower surface area and thus interface area with the electrolyte will result in less SEI film, which is another reason for the low initial irreversible capacity loss of the synthesized Sn_xSbNi electrode.

The charge/discharge curves of Sn_2SbNi alloy electrode for the first and the following four cycles are shown in Fig. 9. In the initial discharge, the potential drops rapidly to a plateau of 0.8 V, then decreases to 0.01 V gradually. From the second cycle, this potential plateau increases from 0.8 V to around 0.85 V. During the initial discharge process, the Sn_2SbNi alloy electrode undergoes four steps marked A–D in Fig. 9. For lithiation process, SEI film will form firstly on the particle surface before step A during the first cycle and always starts at ca. 1.0 V. Then there is a plateau (step A) around 0.8 V corresponding to the Li insertion into the SnSb alloy and Li_3Sb will also be formed at this potential. The slope from 0.7 to 0.3 V represents the potential dependent formation of various Li–Sn alloys (step B–D), because Sn can form different Li_xSn phases with Li. Furthermore, an apparent plateau below 0.1 V in the initial cycle curve can be detected, which disappears in the following cycles. The decomposition of electrolyte resulted from little impurity reaction should be responsible for the low potential plateau. For delithiation process, these insertion processes are reversible. Li will first be extracted from the Li–Sn alloy (D′, C′ and B′), then from Li–Sb alloy (A′). The Sn_2SbNi composite electrode will be resumed when it is recharged to 1.2 V. However, the formation of the SEI film is irreversible. The potential profiles of batteries become almost overlapping in the following cycles evidently,

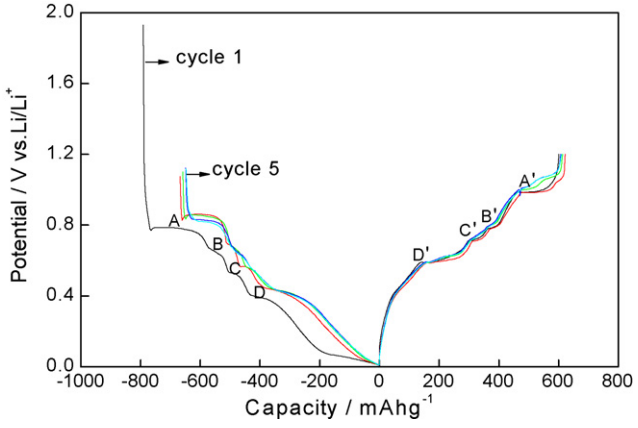

Fig. 9. Charge/discharge curves of Sn_2SbNi composite electrode: the first five cycles.

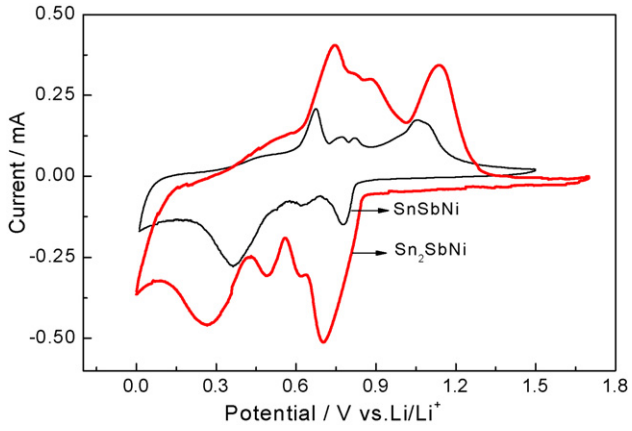

Fig. 10. Plot of cyclic voltammetry of Sn_xSbNi composite electrode with different atomic ratios. The cut-off voltage is 0.1–1.7 V.

illuminating the excellent durability of Sn_2SbNi composite electrode.

Cyclic voltammetry plots of SnSbNi and Sn_2SbNi composite electrode for the 1st cycle are shown in Fig. 10, respectively. Two electrodes show four pairs of peaks, corresponding to the four potential plateaus in charge/discharge curves. With the increase of x value in Sn_xSbNi, the capacity coming from Sn component increases. Meanwhile, the voltage difference between the anodic and cathodic peaks also indicates the relatively growing larger polarization of Sn_2SbNi composite electrode. This should be accountable in part for the slight capacity decline of Sn_2SbNi electrode when compared with SnSbNi electrode. Further investigation concerning the detailed electrochemistry reaction mechanism about Sn_xSbNi composite is in progress.

4. Conclusions

Micro-sized Sn_xSbNi composite anode powders were fabricated by carbothermal reduction from the corresponding oxides of Sn, Sb and Ni. The synthesized spherical Sn_xSbNi particle has a loose structure and is composed of fine grains with different compositions. The space existing in loose particle can accommodate the volume change of electrode during cycling, while the multi-elements characteristic of active material allow the volume change to take place in a stepwise manner. The ductile component Ni will play as a buffer to relieve the volume change stress of electrode. All these factors contribute greatly to the excellent cycling stability of Sn_xSbNi composite electrode.

Increasing the Sn content in Sn_xSbNi composite powder can increase the capacity of composite electrode; however, excessive Sn may cause the electrode fading fast. Sn_2SbNi electrode shows a high reversible specific capacity and an excellent cycleability. The synthesized Sn_xSbNi composite anode powders exhibit a low initial irreversible capacity, mainly due to the low specific surface area of active particles. The excellent electrochemical performance of the micro-scaled SnSbNi composite will serve them as promising anode materials for the new generation of Li-ion batteries.

Acknowledgement

The authors would like to acknowledge financial support provided by 863 Program of National High Technology Research Development Project of China (No. 2006AA03Z231) and National Natural Science Foundation of China (No. 50371007).

References

[1] Y. Idota, T. Kubota, A. Matsufuji, Y. Maekawa, T. Miyasaka, Science 276 (1997) 1395.
[2] I.A. Courtney, J.R. Dahn, J. Electrochem. Soc. 144 (1997) 2045.
[3] M. Winter, J.O. Besenhard, Electrochim. Acta 45 (1999) 31.
[4] J.O. Besenhard, J. Yang, M. Winter, J. Power Sources 68 (1997) 87.
[5] J. Wolfenstine, S. Campos, D. Foster, J. Read, W.K. Behl, J. Power Sources 109 (2002) 230.
[6] H. Zhao, C. Yin, H. Guo, W. Qiu, Electrochem. Solid-State Lett. 2 (2006) 547.
[7] J. Yang, M. Winter, J.O. Besenhard, Solid State Ionics 90 (1996) 281.
[8] J. Yang, Y. Takeda, N. Imanishi, O. Yamamoto, J. Electrochem. Soc. 146 (1999) 4009.
[9] J. Yin, M. Wada, T. Sakai, J. Electrochem. Soc. 150 (2003) A1129.
[10] Y.P. Wu, E. Rahm, R. Holze, J. Power Sources 114 (2003) 228.
[11] I.S. Kim, G.E. Blomgren, P.N. Kumta, Electrochem. Solid-State Lett. 6 (2003) 157.
[12] S.A. Needham, G.X. Wang, H.K. Liu, J. Alloys Compd. 400 (2005) 234.
[13] L.B. Chen, G.Y. Li, Thin Solid Films 462/463 (2004) 395.
[14] H. Li, X.J. Huang, L.Q. Chen, Z.G. Wu, Y. Liang, Electrochem. Solid-State Lett. 2 (1999) 547.
[15] Z.X. Liao, F.Z. Ma, J.H. Hu, Electrochem. Commun. 5 (2003) 657.
[16] M. Wachtler, J.O. Besenhard, M. Winter, J. Power Sources 94 (2001) 189.
[17] J. Yang, Y. Takeda, N. Imanishi, T. Ichikawa, O. Yamamoto, J. Power Sources 79 (1999) 220.
[18] M.J. Lindsay, G.X. Wang, H.K. Liu, J. Power Sources 119 (2003) 84.
[19] S.Z. Zhang, J. Yang, Y.N. Nuli, Solid State Ionics 176 (2005) 693.
[20] A.V. Trifonona, A.A. Momchilov, B.L. Puresheva, I. Abrahams, Solid State Ionics 143 (2001) 319.
[21] D. Larcher, L.Y. Beaulieu, O. Mao, A.E. George, J.R. Dahn, J. Electrochem. Soc. 147 (2000) 1703.
[22] K.D. Keple, J.T. Aughey, M.M. Thackeray, J. Power Sources 81 (1999) 383.
[23] N. Tamura, R. Ohshita, J. Electrochem Soc. 150 (2003) A679.
[24] X.Q. Cheng, P.F. Shi, J. Alloys Compd. 391 (2005) 241.